tvst

Article

Visualization of Mouse Choroidal and Retinal Vasculature Using Fluorescent Tomato Lectin Perfusion

Chunhua Jiao[1,2], Kelsey Adler[3], Xiuying Liu[1,2], Weize Sun[1,2], Robert F. Mullins[1,3], and Elliott H. Sohn[1,3]

[1] Department of Ophthalmology and Visual Sciences, University of Iowa Hospitals & Clinics, Iowa City, IA, USA
[2] Institute for Vision Research, Iowa City, IA, USA
[3] Carver College of Medicine, University of Iowa, Iowa City, IA, USA

Correspondence: Elliott H. Sohn, Department of Ophthalmology, 200 Hawkins Drive, University of Iowa Hospital and Clinics, Iowa City, IA 52242, USA. e-mail: elliott.sohn@gmail.com

Received: September 4, 2019
Accepted: November 27, 2019
Published: January 29, 2020

Keywords: choriocapillaris; retinal vasculature; lectins

Citation: Jiao C, Adler K, Liu X, Sun W, Mullins RF, Sohn EH. Visualization of mouse choroidal and retinal vasculature using fluorescent tomato lectin perfusion. Trans Vis Sci Tech. 2020;9(1):1, https://doi.org/10.1167/tvst.9.1.1

Purpose: To develop a reliable and simplified method to assess choroid and retinal vasculature on whole mount and cross sections in mice using tomato lectin (TL; *Lycopersicon esculentum*).

Methods: Albino mice ($n = 27$) received 1 mg/mL of TL (conjugated to Dylight-594) intravascularly through the tail vein, jugular vein, or cardiac left ventricle. Whole mounts of the retina and choroid were evaluated using fluorescence microscopy. Perfusion with GSL-IB4 conjugated to Dylight-594 and fluorescein isothiocyanate was performed to compare against labeling with TL. Co-labeling of choroidal endothelial cells with perfused TL on cross-sections with antibodies directed against the choriocapillaris-restricted endothelial cell marker CA4 was performed. The percentage of perfused choroidal and retinal vessels was assessed semiquantitatively. One mouse was subjected to thermal laser damage before perfusion to cause retinal and choroidal vasculature ablation.

Results: Intravascular injection of TL led to consistent, robust labeling of retinal and choroidal vascular walls. On cross-sections, choriocapillaris was co-labeled with CA4 and TL. On flat mount, TL perfusion resulted in better labeling of choroidal vessels using tail/jugular vein injection compared with cardiac perfusion ($P < .01$). More consistent labeling of the choroidal and retinal vascular trees was observed with TL than with GSL-IB4. Vascular damage caused by laser ablation was detected readily using this method.

Conclusions: TL injection intravascularly can reliably label normal and ablated choroid and retinal vasculature in mouse in a quick, simple manner.

Translational Relevance: These data will help to facilitate modeling in rodents for diseases such as age-related macular degeneration, diabetes, and other ischemic/angiogenic processes that can also be used for treatment evaluation.

Introduction

There is mounting evidence that damage to the choroidal vasculature, the blood supply for the retinal pigment epithelium and outer retina, plays a key role in the pathogenesis of age-related macular degeneration (AMD)[1–5] and is altered in other diseases such as diabetic retinopathy, central serous retinopathy, and myopia.[6–10] There are relatively robust methods for evaluating morphometric abnormalities of the choroid in humans using histology and fluorescent labeling of donor eyes that can discriminate between intact and ghost vessels[1,2,11–14] as well as in vivo imaging techniques such as optical coherence tomography and optical coherence tomography angiography.[15–17] Such rapid and reliable methods for evaluating the choroid in mice are more challenging especially for whole mount, en face visualization. Current methods (most of which are compared in this article) to histologically

visualize this critical structure using flat mounts in mice result in incomplete labeling of choroidal capillaries, have nonspecific staining, are outside the visible spectrum, or are highly time and/or resource consuming.

Lectins are carbohydrate-binding proteins that are ubiquitous in nature. They are highly specific for specific sugar moieties of protein and lipid glycoconjugates and are commonly used in ocular biology to label various cells in the retina of humans and rodents.[14,18–23] Commonly used lectins for fluorescent labeling of retinal vessels include *Ulex europaeus* agglutinin I or *Griffonia simplicifolia* lectin I isolectin B4 (GSL-IB4) on cross sections or flat mounts via staining or perfusion.[20,23–25] Although *Ulex europaeus* agglutinin I strongly labels blood vessels in human tissues, rodents do not express ligands for *Ulex europaeus* agglutinin I on their blood vessel walls,[26,27] so this lectin is not suitable for animal models. Tomato lectin (TL; *Lycopersicon esculentum* agglutinin) recognizes poly-*N*-acetyl lactosamine–type oligosaccharide moieties[28,29] that is relatively specific for microvessels[30–33] in mice.[34,35] We are not aware of any published reports of TL perfusion for the assessment of normal choroidal vasculature in flat mounts, but it has been described for hyaloidal vessel analysis and choroidal neovascularization detection in the subretinal space.[36–39]

Having a method to readily visualize choroidal and retinal vessels in animals is important to assess models of ocular diseases such as AMD. In this article, we describe a reliable, robust method for visualizing choroidal, choriocapillaris, and retinal vessels on whole mount and cross-sections using a relatively low dose of perfused TL conjugated to fluorescent DyLight-594 in albino mice. Perfusion of this fluorescent TL also allowed visualization of choroid and retina in both normal and mice lasered to cause vessel ablation.

Methods

All animal experiments were performed in accordance with the Association for Research in Vision and Ophthalmology statement for the use of animals in ophthalmic and visual research, and with approval of the University of Iowa Office of Institutional Animal Care and Use Committee. Adult albino mice, B6(CG)-TyrC-2J/J ($n = 13$), BALB/CJ ($n = 10$), and BALB/CBJ ($n = 4$) were purchased from the Jackson Laboratory (Bar Harbor, ME).

Vessel Labeling with TL

Mice were deeply anesthetized by intraperitoneal injection of ketamine (87.5 mg/kg) and xylazine (12.5 mg/kg). A heating pad was used to maintain physiologic body temperature during these procedures. A 6-0 Vicryl suture was placed at the superior pole (12 o'clock) in sclera/choroid to assist with orientation during flat mount. Fluorochrome Dylight 594-conjugated TL (*Lycopersicon esculentum* agglutinin; Vector Laboratories, Burlingame, CA) was used at 100 to 200 µL (1 mg/mL) per mouse by injection into the tail vein or jugular vein of the mouse using a 1-mL syringe equipped with a 32-gauge needle (TSK, Tochiji, Japan) over approximately 15 to 30 seconds (slow delivery being necessary to avoid cardiac arrest). In double-labeling experiments ($n = 2$), a mixture of equal amounts of fluorescent Dylight-594 conjugated TL (100-150 µL at 1 mg/mL) and fluorescein isothiocyanate (FITC)-conjugated GSL-IB4 (100–150 µL at 1 mg/mL) was injected into the tail vein or jugular vein. To ensure that the higher background seen with GSL-IB4 was not due to use of FITC, a similar experiment was performed with a mixture of equal amounts of perfused FITC-conjugated TL (100–150 µL at 1 mg/mL) and fluorescent Dylight 594-conjugated GSL-IB4 (100–150 µL at 1 mg/mL). For intracardiac injection, the anesthetized mice were secured on a platform. After opening the rib cage, the lectin was administered by a 21-gauge needle through the left ventricle, then incubated for 5 minutes. Mice were then perfused transcardially with 10 mL of ice-cold 4% paraformaldehyde using an electric pump (New Era Pump Systems, Farmingdale, NY) connected to a 21-gauge butterfly needle (BD Company, Franklin Lakes, NJ) at a 2 mL/min pump rate. The eyes were immediately extracted and fixed overnight in 4% paraformaldehyde (PFA) in phosphate-buffered saline (PBS) at 4°C.

Flat-mount Preparations and Digital Images

The mouse eyes were enucleated at designated time points and immersed in 4% paraformaldehyde in PBS overnight at 4°C. After the eyeballs were rinsed in 0.1 mol/L of PBS, the anterior chamber, lens, and vitreous were trimmed off without removing the suture. The retinas were carefully separated from the eyecup and optic nerve, and the posterior eye segment containing the sclera–choroid complex and retina were dissected into quarters by four radial cuts with a suture at 12 o'clock and a punch hole at 6 o'clock. Tissues were whole mounted on slides with mounting medium followed by cover slipping. Flat mounts

Table. Comparison of Vessel Labeling Extent Using TL via Intravenous vs. Transcardiac Perfusion with Two Masked, Manual Graders

	Intravenous		Transcardiac	
Grade	Choroid ($n = 10$)	Retina ($n = 10$)	Choroid ($n = 13$)	Retina ($n = 6$)
Excellent (3)	10	10	2	6
Moderate (2)	0	0	9	0
Mild/Poor (1)	0	0	2	0

were examined with a fluorescence microscope (BX51; Olympus, Melville, NY) or confocal microscopes (LSM 710, Zeiss, Thornwood, NY). Images were assessed using Fiji software (http://fiji.sc/Fiji).

Tissue Processing and Immunohistochemistry

After eyes were fixed in 4% PFA overnight at 4°C, the cornea and lens were gently removed, all eyes were cryoprotected through serial sucrose solutions, then embedded in optimal cutting temperature compound (Lab-Tek, Torrance, CA) and frozen in liquid nitrogen. Transverse 10 µm cryosections were collected and mounted on Superfrost Plus glass slides and kept at –80°C until use. Sections were thawed and air dried at room temperature, then blocked in 2% bovine serum albumin/0.5% Triton-X-100 (Sigma, St Louis, MO) for 1 hour at room temperature. Primary antibodies directed against carbonic anhydrase IV (CA4, R&D Systems, Minneapolis, MN; catalog number AF2414, goat anti-mouse IgG) were applied to sections at a concentration of 2 µg/mL in 0.1% Triton + 0.1% bovine serum albumin in 1× PBS and incubated overnight at 4°C. Cy2-conjugated secondary antibody (Jackson Immuno Research Lab, West Grove, PA) was incubated for 1 hour at room temperature at a concentration of 7.5 µg/mL to visualize CA4-positive cells. Sections were washed three times in 1× PBS, and were cover slipped in antifade Vectashield mounting medium with DAPI (Vector Laboratories). For GSL-IB4 or TL staining on cryosections, fluorescently conjugated lectins were incubated for 1 hour at room temperature or overnight at 4°C. All specimens were examined and captured using fluorescence microscopy.

Assessment of Perfusion Extent in Choroid and Retina

To assess whether there was a difference between the extent of vessel labeling with intravenous versus transcardiac injection, the choroid and retina were prelabeled with fluorescent Dylight 594 conjugated TL by perfusion as described elsewhere in this article. Whole mounts of choroid and retina were imaged using a fluorescence microscope (BX51; Olympus). The amount of vessel labeling with TL was graded on a single-digit decimal scale based on the extent of perfusion: 3 (excellent, nearly 100% perfusion of vessels), 2 (moderate), 1 (poor, <10% of possible vessels perfused) based on each quadrant of choroid or retina by two masked, independent graders (Table). Semiautomated measurement was also performed to estimate the percentage of successful positive labeling in a quantitative manner on vessels of choroid and retina in Fiji. The average score was taken of the four quadrants for the two graders. The intraclass correlation coefficient was used to measure the reliability of the estimation among the two graders with the 95% confidence interval.

Mouse Model of Thermal Laser Ablation

Ablation was induced by laser photocoagulation with an Oculight SL/SLx 810nm laser system (Iridex, Mountain View, CA). One adult albino mouse was anesthetized with an intraperitoneal injection of 87.5 mg/kg ketamine and 12.5 mg/kg xylazine. The pupils were dilated with topical 1% tropicamide solution (Akorn, Lake Forest, IL), both eyes were administered genteal gel and covered by 18-mm coverslips. Laser photocoagulation (spot size, 0.5 mm; intensity, 1500 mW; duration, 6000 ms) was performed with one application in the superior fundus. The mouse was humanely killed 24 hours later.

Statistical Analysis

Statistical analysis was performed in GraphPad prism 8 (GraphPad Software, La Jolla, CA). Data were assumed to be normally distributed and were assessed at a confidence interval of 95%. Differences were analyzed with two-tailed unpaired Student *t*-test. Data are presented as mean ± standard deviation and *P* values of less than 0.05 were considered statistically significant.

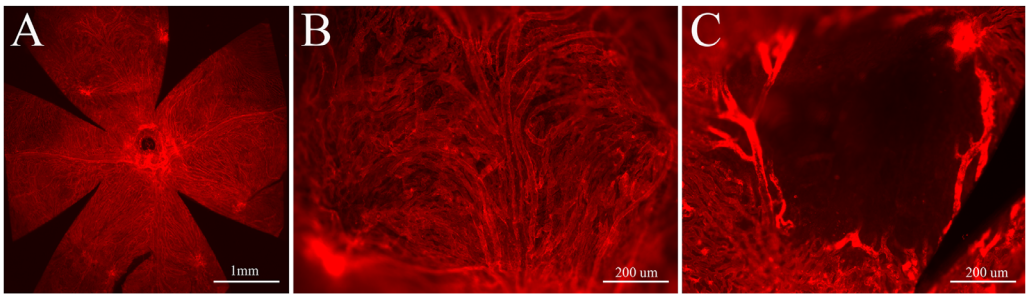

Figure 1. Choroid flat mounts of mice (B6[CG]-TyrC-2J/J) perfused with Dy594-conjugated TL (in *red*). (A) Low magnification image (collected with a 2× objective lens) of normal albino mouse with optic nerve in the center. (B) Higher magnification image collected with a 10× objective lens showing detailed view of normal choroid and choriocapillaris. (C) High magnification microscopic image showing well-demarcated area of focal, central ablation of choroid and choriocapillaris corresponding to the lasered area surrounded by relatively preserved vessels.

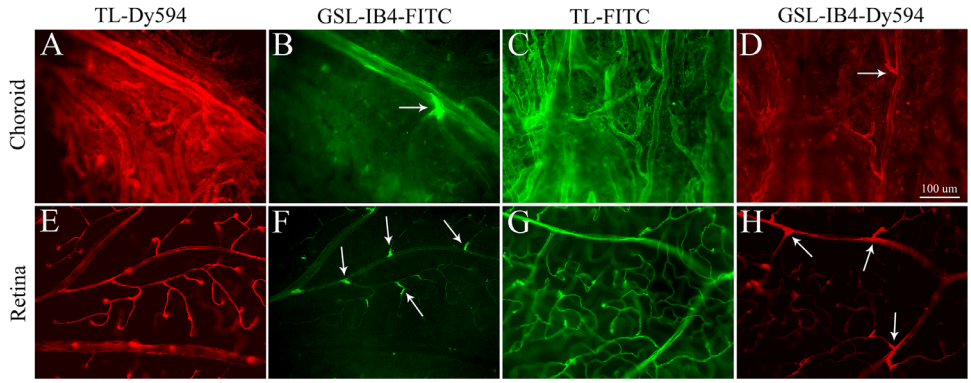

Figure 2. Choroid and retina flat mounts in mouse (BALB/CJ) perfused simultaneously with 100 µL of TL and 100 µL of GSL-IB4 conjugated to different fluorescent antibodies. (A–D) Choroid flat mount images of (A) TL conjugated to Dy594 showing clear delineation of choroidal and choriocapillaris vessels, (B) GSL-IB4 conjugated to FITC with choriocapillaris details obscured, (C) TL conjugated to FITC showing clear delineation of vessels, and (D) GSL-IB4 conjugated to Dy594 demonstrating relatively nonuniform staining of vessels. (E–H) Retinal flat mount images of (E) TL conjugated to Dy594, (F) GSL-IB4 conjugated to FITC, (G) TL conjugated to FITC, and (H) GSL-IB4 conjugated to Dy594. Note the increased signal intensity of GSL-IB4 at vascular branching points (*arrows*) in B, D, F, and H with relative absence of staining in the smaller vessels compared with more uniform staining of all vessels using TL perfusion in A, C, E, and G.

Results

Choroidal Vessel Labeling with TL

After perfusion with TL, there was consistent, robust labeling of choroidal vessels that could be observed at low and high magnification with fluorescence microscopy in normal animals (Figs. 1A and B) with clear delineation of loss in the region of the choroid where laser was applied (Fig. 1C). Because GSL-IB4 perfusion is commonly used to examine retinal vessels on whole mounts, we examined its use for choroidal visualization and found increased labeling at branch points in the choroid and retina with less reliable labeling along the full length of capillary segments (Figs. 2B, 2D, 2F, and 2H) when conjugated to FITC or Dy594 which limits its usefulness; in contrast, with TL perfusion there was more uniform, consistent labeling of choroidal and retinal vessels with Dy594 or FITC (Figs. 2A, 2C, 2E, and 2G).

As expected, TL and GSL-IB4 labeled similar vessels in the choroid and retina, but to ensure that TL had specificity for choroidal vessels, we used a choriocapillaris restricted, endothelial cell-specific marker, CA4,[40,41] to immunolabel cross-sections of mouse eyes that were perfused with TL. Figure 3 demonstrates the relative high specificity of CA4 for choriocapillaris vessels and co-labeling of these vessels with TL. There was no positive staining using secondary antibody alone (Cy2 anti-goat IgG) on cross sections (Fig. 3D).

Retinal Vessel Labeling with TL

After perfusion with TL, there was highly robust, consistent, uniform labeling of retinal vessels at low

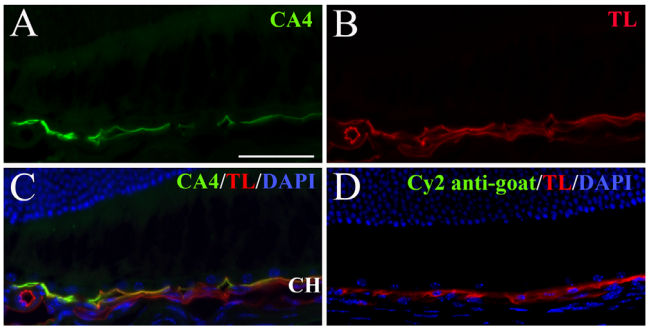

Figure 3. Immunofluorescent-labeled cross-sections with the choriocapillaris enriched CA4 (in *green*) of mouse (B6[CG]-TyrC-2J/J) choroid perfused with Dy594-conjugated TL (in *red*). (A) Labeling of choriocapillaris by CA4 immunofluorescent marker. (B) Labeling of choriocapillaris and larger choroid vessels by TL perfusion. (C) Merged image of perfused TL showing co-labeling with CA4 in the choriocapillaris. (D) Merged image with no primary antibody control demonstrating no positive staining of the choriocapillaris with secondary antibody (Cy2 anti-goat) alone. CA4, carbonic anhydrase IV; DAPI, 4′,6-diamidino-2-phenylindole; CH, choroid

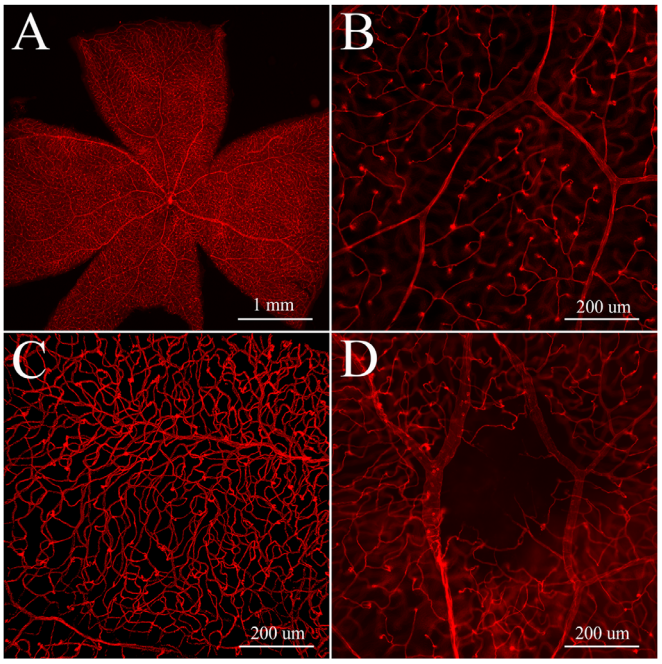

Figure 4. Retinal flat mounts of mouse (B6[CG]-TyrC-2J/J) perfused with Dy594-conjugated TL (in *red*). (A) Low magnification fluorescence microscopic image of normal albino mouse with optic nerve in the center. (B) High magnification fluorescence microscopic image showing detailed view of normal retinal vessels, some not in focus owing to limitations of the microscope. (C) High magnification confocal projection yielding better visualization of all retinal vessels. (D) High magnification microscopic image showing well-demarcated area of focal, central ablation of the retina corresponding with lasered area surrounded by relatively preserved vessels.

and high magnifications (Figs. 2E, 2G, 4A, and 4B) with clear delineation of loss when laser was applied to normal animals (Fig. 4D). When the same dosage of TL and GSL-IB4 were used in combination to perfuse mice, there was a high correspondence of retinal vessel staining between the two, but TL had more uniform staining of entire retinal vessels, whereas GSL labeling was concentrated at endothelial cells of vascular branchpoints (*arrows* in Fig. 2).

Because there are multiple layers of retinal blood vessels with superficial and deep capillary plexi,[20] there are some retinal vessels out of focus on the flat mount owing to limitations of the fluorescence microscope seen in Figures 4A and B. Figure 4C is a projection that shows all of layers of retinal vessels compressed into one two-dimensional image. Supplemental Video S1 shows a three-dimensional representation of retinal vessels imaged with the confocal microscope. A colored rainbow projection image (Supplementary Fig. S1) created using the z-stacked confocal images illustrates the depth of retinal vessels with TL perfusion.

Optimal Perfusion Method for Retinal and Choroidal Flat-mount Visualization

Because transcardiac and intravenous methods are commonly used for perfusion, we compared the rate of labeling for choroidal and retinal vessel visualization on flat mount between these two methods using a semiquantitative assessment by two masked graders (summarized in Table and depicted with average grading values by quadrant in Supplementary Fig. S2). TL perfusion resulted in excellent labeling of choroidal vessels using tail/jugular vein ($n = 10$) injection compared with that of cardiac perfusion ($n = 13$; $P < .001$). Of the mice perfused with TL intravenously, 100% reached excellent vessel labeling in the choroid. In contrast, when perfusing via a transcardiac approach, 15% of mice (2 of 13) had excellent choroidal vessel labeling, 69% of mice showed moderate amount of choroidal vessel labeling, and 15% had poor vessel labeling in the choroid. Labeling of choroidal vessels using the intravenous approach had a standard deviation of 0.052 compared with 0.145 with the transcardiac method. The magnitude of difference between the two standard deviation values show that choroid labeling by intravenous injection had smaller variability than transcardiac perfusion. In addition, semiautomated quantification of vessels using Fiji show significantly better ($P < .01$) vessel labeling in the choroid using intravenous injection compared with transcardiac perfusion; a trend ($P = .07$) toward improved labeling was seen in

the retina of those given intravenous compared with transcardiac perfusion (Supplementary Fig. S3). Thus, both semiquantitative assessments using masked, manual graders and semiautomated quantification after thresholding in Fiji yielded better choroidal visualization with intravenous perfusion compared with the transcardiac approach.

Discussion

In this article, we describe a simplified method of perfusing conjugated TL to reliably assess choroidal and retinal vasculature using whole-mount and cross-section analyses in mice. We found this method to be better than perfusion with another commonly used lectin, GSL-IB4, for choroidal flat mounts. The labeling for retinal vessels is as robust as GSL-IB4, but may be preferred over GSL-IB4 owing to the lower concentration needed for adequate staining in addition to more uniform staining of vessels observed with TL. The advantage of looking at choroidal and retinal flat mounts with conjugated TL was further demonstrated with a laser model of ablation in normal mice.

Although there are multiple approaches for evaluating retinal vessels on whole mounts in rodents that can be used for different purposes (including confirmation of TL for retinal vessels as shown by other groups[37,42]), methods to rapidly evaluate choroidal vasculature defects in rodents are relatively limited. In this study, we found comparable staining of choroidal (and retinal) vessels using perfused TL to GSL-IB4 with better visualization of vessels using TL on whole mount sections. Other methods assessed in our laboratory that did not provide as compelling and consistent labeling of choroidal flat mounts included: alkaline phosphatase (BCIP/NBT), FITC-albumin, and DiI (Supplementary Table S1). In addition, we observed concentrated endothelial cell labeling with GSL-IB4 (perfused) at vascular branchpoints in both choroidal and retinal vessels with comparatively more uniform labeling of vessels with TL. The concentrated endothelial cell labeling of branchpoints with perfused GSL-IB4 can be contrasted with the mild increase in labeling at small branchpoints seen with perfused TL (e.g., Fig. 4B), which is due to visualization of connections between retinal plexi.

Dual perfusion experiments using the same dose of GSL-IB4 and TL demonstrated weaker signal on retinal whole mounts of GSL-IB4 than TL whether GSL-IB4 or TL was conjugated with FITC or Dy594. One could increase the dose of GSL-IB4 but this increases cost by 5 to 10 times. Our methodology uses a lower dose of TL than GSL-IB4, which results in significantly less expensive experiments.

We observed a high rate of perfusion using intravenous injection of TL, but we recognize that intracardiac injections have also been used previously with excellent results.[33,36,37,43,44] Intravenous injections (tail or jugular vein) resulted in excellent perfusion of choroidal vessels in these animals that was higher than intracardiac injection, so this route of injection is preferred when trying to assess choroidal vasculature. The lower rate of success for vessel visualization with intracardiac perfusion is unclear may be because the thoracotomy can cause inefficient ventilation, respiratory and circulatory dysfunction that has greater impact on the choriocapillaris than retinal vessels.

A potential method for readily visualizing choroidal vasculature in rodents employs the use of optical coherence tomography angiography. This field is gaining more momentum, but at this time a custom-built machine with specialized software is needed for analysis of data.[45] A clear advantage of an optical coherence tomography-based imaging method is its in vivo nature, but even in humans this is still a nascent technology. There are inherent limitations of using optical coherence tomography angiography for choroidal analysis, such as evaluating specific cell and molecular biological effects that can only be realized with histologic methods, but there is hope that coherence tomography angiography–based imaging can be used to better visualize the choroid in rodents in the future. Additionally, in vivo molecular imaging techniques are also in development.[46]

Future studies with this model will allow rapid assessment of perfusion defects and potential therapies[47,48] that are selective to the choroid or retina using flat mount sections and analysis using cross-section staining.

Acknowledgments

We thank Jian Q. Shao from the Central Microscopy Research Facility for assisting with the confocal microscopy imaging. We also thank Miles Flamme-Wiese for his technical assistance.

Supported by NIH Grants R01 EY026547 and P30 EY025580; and the Elmer and Sylvia Sramek Charitable Foundation.

Disclosure: **C. Jiao,** None; **K. Adler,** None; **X. Liu,** None; **W. Sun,** None; **R.F. Mullins,** None; **E.H. Sohn,** Oxford Biomedica (F); none relevant to this study

References

1. Sohn EH, Flamme-Wiese MJ, Whitmore SS, et al. Choriocapillaris degeneration in geographic atrophy. *Am J Pathol*. 2019;189:1473–1480. doi:10.1016/j.ajpath.2019.04.005.
2. Mullins RF, Schoo DP, Sohn EH, et al. The membrane attack complex in aging human choriocapillaris: relationship to macular degeneration and choroidal thinning. *Am J Pathol*. 2014;184:3142–3153. doi:10.1016/j.ajpath.2014.07.017.
3. Whitmore SS, Sohn EH, Chirco KR, et al. Complement activation and choriocapillaris loss in early AMD: implications for pathophysiology and therapy. *Prog Retin Eye Res*. 2015;45:1–29. doi:10.1016/j.preteyeres.2014.11.005.
4. Sohn EH, Khanna A, Tucker BA, Abràmoff MD, Stone EM, Mullins RF. Structural and biochemical analyses of choroidal thickness in human donor eyes. *Invest Ophthalmol Vis Sci*. 2014;55:1352–1360. doi:10.1167/iovs.13-13754.
5. Seddon JM, McLeod DS, Bhutto IA, et al. Histopathological insights into choroidal vascular loss in clinically documented cases of age-related macular degeneration. *JAMA Ophthalmol*. 2016;134:1272–1280. doi:10.1001/jamaophthalmol.2016.3519.
6. Regatieri CV, Branchini L, Carmody J, Fujimoto JG, Duker JS. Choroidal thickness in patients with diabetic retinopathy analyzed by spectral-domain optical coherence tomography. *Retina (Philadelphia, Pa)*. 2012;32:563–568. doi:10.1097/IAE.0b013e31822f5678.
7. Spaide RF. Choriocapillaris flow in myopia. *Invest Ophthalmol Vis Sci*. 2017;58:3563–3564. doi:10.1167/iovs.17-22042.
8. Spaide RF. DITORIALThe Choroid and Vision Loss. *Am J Ophthalmol*. 2014;158:649–650. doi:10.1016/j.ajo.2014.07.001.
9. Kuroda S, Ikuno Y, Yasuno Y, et al. Choroidal thickness in central serous chorioretinopathy. *Retina (Philadelphia, Pa)*. 2013;33:302–308. doi:10.1097/IAE.0b013e318263d11f.
10. Kim S-W, Oh J, Kwon S-S, Yoo J, Huh K. Comparison of choroidal thickness among patients with healthy eyes, early age-related maculopathy, neovascular age-related macular degeneration, central serous chorioretinopathy, and polypoidal choroidal vasculopathy. *Retina (Philadelphia, Pa)*. 2011;31:1904–1911. doi:10.1097/IAE.0b013e31821801c5.
11. Seddon JM, McLeod DS, Bhutto IA, et al. Histopathological insights into choroidal vascular loss in clinically documented cases of age-related macular degeneration. *JAMA Ophthalmol*. 2016;134:1272–1280. doi:10.1001/jamaophthalmol.2016.3519.
12. Li M, Huisingh C, Messinger J, et al. Histology of geographic atrophy secondary to age-related macular degeneration: a multilayer approach. *Retina (Philadelphia, Pa)*. 2018;38:1937–1953. doi:10.1097/IAE.0000000000002182.
13. Sohn EH, Chirco KR, Folk JC, Mullins RF. Clinicopathological correlation in a patient with previously treated birdshot chorioretinopathy. *Retin Cases Brief Rep*. 2017;11:344–347. doi:10.1097/ICB.0000000000000367.
14. Sohn EH, Flamme-Wiese MJ, Whitmore SS, Wang K, Tucker BA, Mullins RF. Loss of CD34 expression in aging human choriocapillaris endothelial cells. *PLoS ONE*. 2014;9:e86538. doi:10.1371/journal.pone.0086538.
15. Lee SY, Cheng JL, Gehrs KM, et al. Choroidal features of acute macular neuroretinopathy via optical coherence tomography angiography and correlation with serial multimodal imaging. *JAMA Ophthalmol*. 2017;135:1177–1183. doi:10.1001/jamaophthalmol.2017.3790.
16. Zhang L, Buitendijk GHS, Lee K, et al. Validity of automated choroidal segmentation in SS-OCT and SD-OCT. *Invest Ophthalmol Vis Sci*. 2015;56:3202–3211. doi:10.1167/iovs.14-15669.
17. Oguz I, Abràmoff MD, Zhang L, Lee K, Zhang EZ, Sonka M. 4D graph-based segmentation for reproducible and sensitive choroid quantification from longitudinal OCT scans. *Invest Ophthalmol Vis Sci*. 2016;57:OCT621–OCT630. doi:10.1167/iovs.15-18924.
18. Mullins RF, Hageman GS. Human ocular drusen possess novel core domains with a distinct carbohydrate composition. *J Histochem Cytochem*. 1999;47:1533–1540. doi:10.1177/002215549904701205.
19. Mullins RF, Johnson LV, Anderson DH, Hageman GS. Characterization of drusen-associated glycoconjugates. *Ophthalmology*. 1997;104:288–294. doi:10.1016/S0161-6420(97)30322-4.
20. Sohn EH, van Dijk HW, Jiao C, et al. Retinal neurodegeneration may precede microvascular changes characteristic of diabetic retinopathy in diabetes mellitus. *Proc Natl Acad Sci USA*. 2016;113:E2655–E2664. doi:10.1073/pnas.1522014113.

21. Smith LE, Wesolowski E, McLellan A, et al. Oxygen-induced retinopathy in the mouse. *Invest Ophthalmol Vis Sci*. 1994;35:101–111.
22. Rudolf M, Malek G, Messinger JD, Clark ME, Wang L, Curcio CA. Sub-retinal drusenoid deposits in human retina: organization and composition. *Exp Eye Res*. 2008;87:402–408. doi:10.1016/j.exer.2008.07.010.
23. Vinores SA, Derevjanik NL, Ozaki H, Okamoto N, Campochiaro PA. Cellular mechanisms of blood-retinal barrier dysfunction in macular edema. *Doc Ophthalmol*. 1999;97:217–228.
24. Park SE, Mieler WF, Pulido JS. 2 peripheral scatter photocoagulation for neovascularization associated with pars planitis. *Arch Ophthalmol*. 1995;113:1277–1280.
25. Saint-Geniez M, Kurihara T, Sekiyama E, Maldonado AE, D'Amore PA. An essential role for RPE-derived soluble VEGF in the maintenance of the choriocapillaris. *Proc Natl Acad Sci U S A*. 2009;106:18751–18756. doi:10.1073/pnas.0905010106.
26. Alroy J, Goyal V, Skutelsky E. Lectin histochemistry of mammalian endothelium. *Histochemistry*. 1987;86:603–607.
27. Debbage PL. A systematic histochemical investigation in mammals of the dense glycocalyx glycosylations common to all cells bordering the interstitial fluid compartment of the brain. *Acta Histochem*. 1996;98:9–28. doi:10.1016/S0065-1281(96)80046-8.
28. Kawashima H, Sueyoshi S, Li H, Yamamoto K, Osawa T. Carbohydrate binding specificities of several poly-N-acetyllactosamine-binding lectins. *Glycoconj J*. 1990;7:323–334.
29. Zeng X, Murata T, Kawagishi H, Usui T, Kobayashi K. Analysis of specific interactions of synthetic glycopolypeptides carrying N-acetyllactosamine and related compounds with lectins. *Carbohydr Res*. 1998;312:209–217.
30. Porter GA, Palade GE, Milici AJ. Differential binding of the lectins Griffonia simplicifolia I and Lycopersicon esculentum to microvascular endothelium: organ-specific localization and partial glycoprotein characterization. *Eur J Cell Biol*. 1990;51:85–95.
31. Rymer CC, Sims-Lucas S. In utero intra-cardiac tomato-lectin injections on mouse embryos to gauge renal blood flow. *J Vis Exp*. 2015;96:e52398. doi:10.3791/52398.
32. Manalo T, May A, Quinn J, et al. Differential lectin binding patterns identify distinct heart regions in giant Danio (Devario aequipinnatus) and Zebrafish (Danio rerio) hearts. *J Histochem Cytochem*. 2016;64:687–714. doi:10.1369/0022155416667928.
33. Robertson RT, Levine ST, Haynes SM, et al. Use of labeled tomato lectin for imaging vasculature structures. *Histochem Cell Biol*. 2015;143:225–234. doi:10.1007/s00418-014-1301-3.
34. Peña LA, Fuks Z, Kolesnick RN. Radiation-induced apoptosis of endothelial cells in the murine central nervous system: protection by fibroblast growth factor and sphingomyelinase deficiency. *Cancer Res*. 2000;60:321–327.
35. Thurston G, Baluk P, Hirata A, McDonald DM. Permeability-related changes revealed at endothelial cell borders in inflamed venules by lectin binding. *Am J Physiol*. 1996;271:H2547–H2562. doi:10.1152/ajpheart.1996.271.6.H2547.
36. Hara R, Inomata Y, Kawaji T, et al. Suppression of choroidal neovascularization by N-acetylcysteine in mice. *Curr Eye Res*. 2010;35:1012–1020. doi:10.3109/02713683.2010.500112.
37. Watson EC, Koenig MN, Grant ZL, et al. Apoptosis regulates endothelial cell number and capillary vessel diameter but not vessel regression during retinal angiogenesis. *Development*. 2016;143:2973–2982. doi:10.1242/dev.137513.
38. Montezuma SR, Dolezal LD, Rageh AA, Mar K, Jordan M, Ferrington DA. Lactoferrin reduces chorioretinal damage in the murine laser model of choroidal neovascularization. *Curr Eye Res*. 2015;40:946–953. doi:10.3109/02713683.2014.969808.
39. Mitsuhashi J, Morikawa S, Shimizu K, Ezaki T, Yasuda Y, Hori S. Intravitreal injection of erythropoietin protects against retinal vascular regression at the early stage of diabetic retinopathy in streptozotocin-induced diabetic rats. *Exp Eye Res*. 2013;106:64–73. doi:10.1016/j.exer.2012.11.001.
40. Giacalone JC, Miller MJ, Workalemahu G, et al. Generation of an immortalized human choroid endothelial cell line (iChEC-1) using an endothelial cell specific promoter. *Microvasc Res*. 2018;123:50–57. doi:10.1016/j.mvr.2018.12.002.
41. Baba T, Grebe R, Hasegawa T, et al. Maturation of the fetal human choriocapillaris. *Invest Ophthalmol Vis Sci*. 2009;50:3503–3511. doi:10.1167/iovs.08-2614.
42. Campa C, Kasman I, Ye W, Lee WP, Fuh G, Ferrara N. Effects of an anti-VEGF-A monoclonal antibody on laser-induced choroidal neovascularization in mice: optimizing methods to quantify vascular changes. *Invest Ophthalmol Vis Sci*. 2008;49:1178–1183. doi:10.1167/iovs.07-1194.
43. Ablonczy Z, Dahrouj M, Marneros AG. Progressive dysfunction of the retinal pigment

epithelium and retina due to increased VEGF-A levels. *FASEB J*. 2014;28:2369–2379. doi:10.1096/fj.13-248021.
44. Dickie R, Bachoo RM, Rupnick MA, et al. Three-dimensional visualization of microvessel architecture of whole-mount tissue by confocal microscopy. *Microvasc Res*. 2006;72:20–26. doi:10.1016/j.mvr.2006.05.003.
45. Zhi Z, Yin X, Dziennis S, et al. Optical microangiography of retina and choroid and measurement of total retinal blood flow in mice. *Biomed Opt Express*. 2012;3:2976–2986. doi:10.1364/BOE.3.002976.
46. Feenstra DJ, Seleci M, Denk N, Fauser S, Drawnel FM, Jayagopal A. Indocyanine green molecular angiography of choroidal neovascularization. *Exp Eye Res*. 2019;180:122–128. doi:10.1016/j.exer.2018.12.016.
47. Zeng S, Wen K-K, Workalemahu G, et al. Imidazole compounds for protecting choroidal endothelial cells from complement injury. *Sci Rep*. 2018;8:13387. doi:10.1038/s41598-018-31846-z.
48. Zeng S, Whitmore SS, Sohn EH, et al. Molecular response of chorioretinal endothelial cells to complement injury: implications for macular degeneration. *J Pathol*. 2016;238:446–456. doi:10.1002/path.4669.

Supplementary Material

Supplementary Video. Three-dimensional video projection of mouse retina labeled with perfused Dy594-conjugated TL.